

# Evidence that tissue recoil in the early *Drosophila* embryo is a passive not active process

Amanda Nicole Goldner, Salena M. Fessehaye, Nataly Rodriguez, Kelly Ann Mapes, Miriam Osterfield\*, Konstantin Doubrovinski\*

Department of Biophysics and Department of Cell Biology, University of Texas Southwestern Medical Center, Dallas, TX 75390

**ABSTRACT** Understanding tissue morphogenesis is impossible without knowing the mechanical properties of the tissue being shaped. Although techniques for measuring tissue material properties are continually being developed, methods for determining how individual proteins contribute to mechanical properties are very limited. Here, we developed two complementary techniques for the acute inactivation of spaghetti squash (the *Drosophila* myosin regulatory light chain), one based on the recently introduced (auxin-inducible degron 2 (AID2) system, and the other based on a novel method for conditional protein aggregation that results in nearly instantaneous protein inactivation. Combining these techniques with rheological measurements, we show that passive material properties of the cellularization-stage *Drosophila* embryo are essentially unaffected by myosin activity. These results suggest that this tissue is elastic, not predominantly viscous, on the developmentally relevant timescale.

## Monitoring Editor

Dennis Discher  
University of Pennsylvania

Received: Sep 08, 2022

Revised: Jun 26, 2023

Accepted: Jun 28, 2023

## INTRODUCTION

Tissue morphogenesis is at its core a mechanical process, in which changes in tissue shape are directed by spatio-temporal patterns of forces and material properties (Keller, 2012; Davidson, 2017). How the material properties of a tissue – such as elasticity, viscosity, or plasticity – arise from its constituent parts is an area of ongoing investigation. In some tissues, mechanical properties may be dominated by supracellular structures based on extracellular matrix, cell-cell interactions, or cell-interstitial packing (Lenne and Trivedi, 2022). In other tissues, such as simple epithelia with strong cell adhesion, the mechanical properties of cells, and therefore the cytoskeleton, might be expected to dominate tissue properties.

One approach to studying cytoskeletal mechanics involves studies of cytoskeletal gels that have been reconstituted in vitro (Gardel et al., 2008; Joanny and Prost, 2009; Pegoraro et al., 2017). Rheological measurements, combined with theoretical or computational

approaches, have generated insights into the mechanical effects of filament length distribution (Janmey et al., 1994), and the effects of adding crosslinkers or motors (Bendix et al., 2008; Koenderink et al., 2009). However, it can be difficult to directly translate these insights into understanding how cells actually control cytoskeletal mechanics in vivo. This is partially because reconstituted systems generally have fewer distinct components than of in vivo cytoskeletal networks; for example, the number of distinct actin binding proteins in the fly has been estimated to be around 80 (Goldstein and Gunawardena, 2000). Additionally, in vitro gels are usually spatially homogenous, while cytoskeletal networks in cells usually are nonhomogeneous (e.g., the cortex versus the bulk of the cytosol; Van Citters et al., 2006), and can sometimes exhibit exquisite spatial patterning (Xu et al., 2013; Dubey et al., 2020).

A complementary approach has been to conduct mechanical measurements directly on living cells or tissues (Campas et al., 2014; Serwane et al., 2017; Mongera et al., 2018; D'Angelo et al., 2019; Khalilgharibi et al., 2019). These studies are extremely valuable for determining the actual material properties of these complex biological entities. However, studies aimed at understanding the contribution of specific proteins to cell or tissue rheology are much more limited, and have mostly been done with proteins that can be targeted pharmacologically (Van Citters et al., 2006; D'Angelo et al., 2019). To more generally assess the role specific proteins play in tissue mechanics, it is critical to measure tissue mechanics after depleting this protein extremely rapidly. The speed of depletion is important to avoid nonspecific downstream effects, including possibilities ranging from compensatory mechanisms to severe cellular

This article was published online ahead of print in MBoC in Press (<http://www.molbiolcell.org/cgi/doi/10.1091/mbc.E22-09-0409>) on July 5, 2023.

\*Address correspondence to: Konstantin Doubrovinski (Konstantin.Doubrovinski@UTSouthwestern.edu); Miriam Osterfield (Miriam.Osterfield@UTSouthwestern.edu).

Abbreviations used: AID, auxin-inducible degron; FKBP, FK506 binding protein; FRB, FKBP12-rapamycin binding domain; GFP, green fluorescent protein; TIR1, transport inhibitor response 1.

© 2023 Goldner et al. This article is distributed by The American Society for Cell Biology under license from the author(s). Two months after publication it is available to the public under an Attribution–Noncommercial–Share Alike 4.0 International Creative Commons License (<http://creativecommons.org/licenses/by-nc-sa/4.0>).

“ASCB®,” “The American Society for Cell Biology®,” and “Molecular Biology of the Cell®” are registered trademarks of The American Society for Cell Biology.

dysfunction. As a result, techniques such as gene mutation or RNAi are likely to be too slow acting, while protein-based depletion techniques such as induced degradation or sequestration appear more promising (Natsume and Kanemaki, 2017).

A major debate in the field has emerged over whether embryonic tissues are predominantly viscous (Mayer *et al.*, 2010; Behrnt *et al.*, 2012; Munster *et al.*, 2019) or elastic (Dobrovinski *et al.*, 2017; Hernandez-Vega *et al.*, 2017; Vuong-Brender *et al.*, 2017) on the developmentally relevant timescale. A number of recent papers demonstrated that after various embryonic tissues are stretched, they recoil back to the original configuration, suggesting that they are elastic (Bambardekar *et al.*, 2015; Dobrovinski *et al.*, 2017; D'Angelo *et al.*, 2019). However, those observations are consistent with viscosity-dominated models if the recoil is driven by active (notably myosin-generated) force. Distinguishing between these possibilities would require doing the measurements after molecular motors are depleted.

In the first hours of development, the fly embryo is a syncytium in which nuclei share a common cytoplasm as they undergo 13 rounds of division. Subsequently, in the process of cellularization, membranes protrude from the surface of the embryo in between those nuclei to partition the embryo into separate cells, thus forming a stage called the blastula (Campos-Ortega and Hartenstein, 1985). Immediately afterward, the large-scale tissue movements of gastrulation begin. These processes in *Drosophila* have served as a prime model for understanding the molecular and physical mechanisms underlying epithelial morphogenesis (Blankenship *et al.*, 2006; Martin *et al.*, 2009; Kiehart *et al.*, 2017). Additionally, several techniques have been developed to examine the mechanical properties of the early embryo (Bambardekar *et al.*, 2015; Dobrovinski *et al.*, 2017; D'Angelo *et al.*, 2019), making this an ideal system to investigate the contribution of individual cytoskeletal components to tissue rheology.

In this study, we used two complementary techniques to acutely inactivate myosin regulatory light chain (MRLC, called spaghetti squash or sqh in *Drosophila*) in the early *Drosophila* embryo. We chose sqh as our target because MRLC is thought to be required for myosin motor function (Karess *et al.*, 1991; Chen *et al.*, 1994). One of our techniques relies on the recently introduced AID2 system and was optimized to enable depletion after tens of minutes following injection of a drug. The second technique introduced here, relies on conditional aggregation of a green fluorescent protein (GFP)-tagged protein, and operates within minutes. Combining these techniques with our previously developed method to probe material properties of embryonic tissues, we have established that mechanical properties of the early embryo are largely unaffected by sqh depletion. In combination with our previous findings, these results suggest that tissue recoil upon force removal is indeed a signature of elasticity rather than active tension.

## RESULTS

To rapidly deplete the MRLC sqh in the early *Drosophila* embryo, we first used a recently enhanced version of the AID degron system (Nishimura *et al.*, 2009; Yesbolatova *et al.*, 2020). This technique involves translationally fusing the protein of interest to AID (auxin-inducible degron), which binds a plant-derived protein TIR1 (transport inhibitor response 1) upon addition of auxin. Once the AID-TIR1 complex is formed, the AID tag is polyubiquitinated and the AID-fusion protein is targeted for proteasomal degradation. The AID2 system, which we use here, eliminates leaky (auxin-independent) degradation by employing a mutated TIR1 (TIR1<sup>F74G</sup>) and a modified ligand (5-Ph-IAA or 5-Ph-IAA-AM) (Yesbolatova *et al.*, 2020; Negishi *et al.*, 2022).

We first engineered a fly strain where sqh was translationally fused to a shortened AID sequence and GFP at the endogenous locus using CRISPR/Cas9 (Kubota *et al.*, 2013; Morawska and Ulrich, 2013; Brosh *et al.*, 2016; Bence *et al.*, 2017). To decrease the total amount of myosin to be depleted, and thus the expected depletion time, we constructed flies in which the second allele of sqh was a null (sqh<sup>Ax3</sup>). We also overexpressed TIR1<sup>F74G</sup> maternally using two UASp-TIR1<sup>F74G</sup> constructs driven by two copies of mat-GAL4 to further enhance the rate of myosin degradation upon drug application. Finally, the genotype used included a red membrane marker (Gap43-mCherry) to visualize cell outlines.

With this genetic background prepared, we began experiments investigating how myosin activity impacts tissue rheology in the early fly embryo. First, we examined the time-course of myosin depletion upon induction of AID-mediated degradation. Embryos were injected with 5-Ph-IAA-AM ~ 10–15 min before the onset of cellularization, then imaged to monitor the green fluorescence signal from any remaining sqh<sup>GFP-AID</sup>. Over multiple experiments, average fluorescence was found to drop to its minimum within 30–50 min after the injection (Figure 1, a, c, and c'). This minimum level of fluorescence is comparable to autofluorescence, as assessed by imaging embryos expressing Gap43-mCherry but not GFP, indicating that the pool of sqh is overwhelmingly depleted. Images at the level of the basal cellularization front (Figure 1, b and b') show that very faint fluorescence remains detectable in injected embryos at this location. However, basal outlines become markedly wavy and irregular (Figure 1, b and b', insets; see also Supplemental Figure S2a for quantification). This indicates that residual amounts of sqh<sup>GFP-AID</sup> are insufficient to maintain basal tension. Additionally, 5-Ph-IAA-AM-injected embryos reproducibly failed to form ventral furrows or undergo any other gastrulation processes (10/10 embryos), which is also consistent with loss of myosin function (Supplemental Movies 1 and 2). For comparison, 2/10 DMSO-injected controls failed to complete ventral furrow formation. Although the furrow canal appears to lack tension, the cellularization front proceeds normally (unpublished data) in agreement with previously published work (Royou *et al.*, 2004).

Having established a method to rapidly deplete sqh in the early embryo, we asked how this influences material properties of embryonic tissues. To this end, we exploited a previously developed assay for probing tissue rheology using ferrofluid droplets (Dobrovinski *et al.*, 2017). In this assay, a small (10–20 micron) droplet of ferrofluid is first injected into an embryo and positioned in the cellular layer by an externally applied magnet (Figure 2a). The magnet is then rapidly placed near the embryo surface some distance from the ferrofluid droplet, causing the droplet to move toward the magnet and stretching the surrounding cellular layer. In our experiments, we imposed this force-loading phase for approximately 1 min (Figure 2a'). The magnet was then rapidly withdrawn, removing the external magnetic force from the droplet and allowing any subsequent tissue relaxation to be monitored. (Figure 2a'').

We applied this ferrofluid assay multiple times to both control embryos (Figure 2b) and embryos in which sqh was depleted using the AID2 system (Figure 2c). To allow for maximal sqh depletion, ferrofluid pulling experiments were performed 40–60 min after the injection of 5-Ph-IAA-AM. Qualitatively, the observed mechanical responses are essentially indistinguishable. In particular, during the force-loading phase, the displacement of the droplet  $d$  as a function of time is well described by a power law dependence  $d(t) = t^\alpha$ , with  $\alpha \approx 1/2$ , in both the drug-treated embryos as well as in the controls. These results are in close quantitative agreement with previously reported data (Dobrovinski *et al.*, 2017), indicating that the

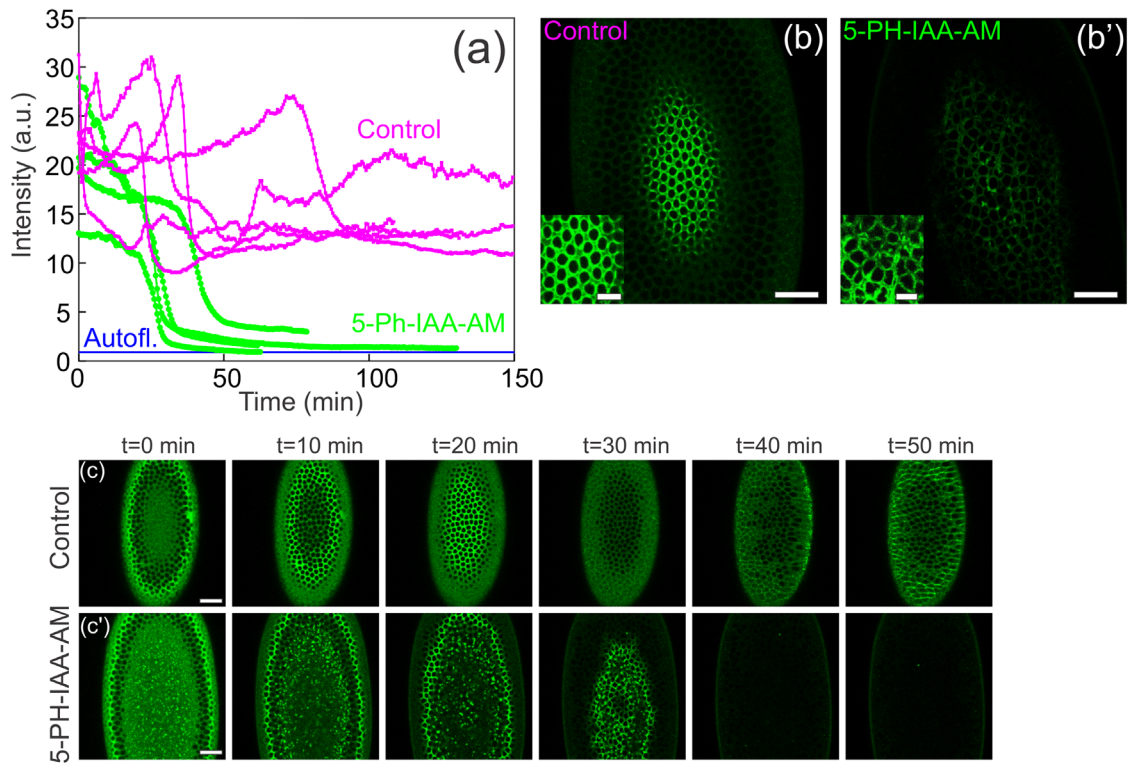


**FIGURE 1:** The kinetics of myosin depletion using the AID2 degron system. (a) The dynamics of myosin depletion quantified as the time-course of fluorescence intensity within a region of interest. (b and b') Myosin fluorescence at the cellularization front in a control embryo and in a 5-Ph-IAA-AM injected embryo at the same time-point in cellularization. Confocal slices were taken 26 microns beneath the surface of the embryo. The main images were taken with the same microscope settings and processed in identical ways. The insets are magnified images, adjusted separately for brightness to allow for easier visualization in the 5-Ph-IAA-AM sample. Scale bars are 25  $\mu\text{m}$  in the main figures and 10  $\mu\text{m}$  in the insets. (c and c') Representative snapshots showing the time-course of  $\text{sqh}^{\text{GFP-AID}}$  depletion. Scalebar: 25  $\mu\text{m}$ .

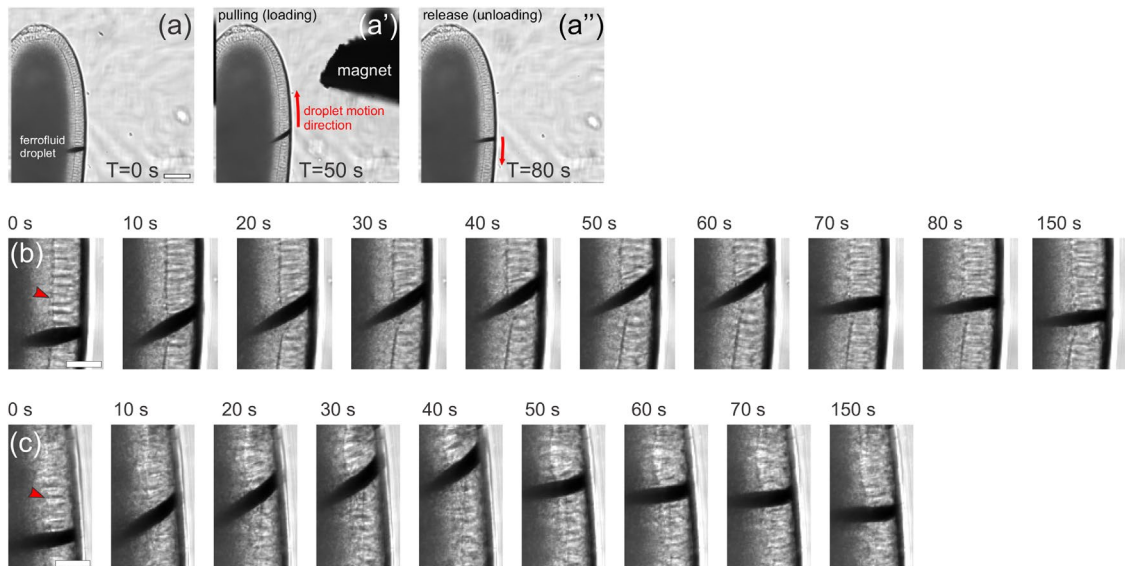


**FIGURE 2:** Ferrofluid-based assay used to quantify tissue material properties in different conditions. (a–a'') Snapshots of the ferrofluid pulling assay performed on untreated (control) embryos. Scalebar: 50  $\mu\text{m}$ . (b and c) Zoomed in regions of interest illustrating the dynamics of the droplet being pulled by the magnet in two experiments. (b) is an uninjected control embryo, while (c) is a 5-Ph-IAA-AM injected  $\text{sqh}^{\text{GFP-AID}}$  embryo. Note that the cellularization front (red arrowhead) is much more apparent in the untreated control case: this is a representative effect of the treatment, making the cellularization front appear “floppy” and uneven. Scalebar: 20  $\mu\text{m}$ .

particular genetic background does not significantly affect tissue material properties.

To compare the two conditions more quantitatively, we calculated characteristic properties that quantify the dynamics in the unloading, or relaxation phase of the assay. One characteristic property is the percent recoil, which reflects the extent to which elastic energy is stored over time. In other words, a system that stores elastic energy perfectly would have 100% recoil, while lower percentages indicate that the system “forgets” its initial state over time. For control experiments, the percent recoil measured  $73.5 \pm 2.1$  SEM ( $n = 9$ ), while the corresponding figure for the sqh-depleted embryos was  $74.8 \pm 2.6$  SEM ( $n = 6$ ), indicating that removal of sqh had no apparent effect on the ability of the tissue to store elastic stress. The other characteristic property we measured was the relaxation time constant (measured as the asymptotic slope of the decay curves in the rightmost plots from Figure 3), which reflects the ratio of elasticity to viscosity of the tissue. The relaxation time constant was  $64.5 \pm 5.0$  (SEM) seconds ( $n = 9$ ) in the control condition, and  $52.8 \pm 5.6$  (SEM) seconds ( $n = 5$ ) for the sqh-depleted embryos. The slight apparent difference in these time constants was not statistically significant (see Figure 3 legend); more importantly, though, it was remarkably small in magnitude. Together these results seem to indicate that the mechanical properties of the tissue are largely independent of sqh.

Although our results from the AID2 degron assay suggest that tissue material properties are not substantially affected by depletion of sqh, we were concerned that the 40-min interval allowed for protein degradation was relatively long and could still allow for downstream compensatory processes to occur. To address this concern, we sought to develop a technique to interfere with sqh on a still faster timescale. We decided to try sequestering our protein into non-functional aggregates. Our first attempt involved endogenously tagging sqh with FRB and GFP, and monitoring the aggregation of sqh upon injection of FK506 binding protein (FRB) and rapamycin. Although the simple combination of FK506 binding protein (FKBP) and rapamycin injected together did not promote significant aggregation of sqh<sup>FRB-GFP</sup> protein (unpublished data), the injection of rapamycin and biotinylated FKBP followed by streptavidin resulted in rapid and pervasive aggregation of sqh<sup>FRB-GFP</sup> in the vicinity of the injection site. Furthermore, this aggregation appeared to deplete sqh activity, because cellularization was markedly slowed and basal rings failed to close in this region (Supplemental Figure S1, a and a').

Inspired by these results, we next attempted to develop a more generally applicable aggregation technique using several layers of multivalent interactions but targeting the GFP tag rather than the FRB tag (Figure 4a). We found that injecting sqh<sup>FRB-GFP</sup> embryos with biotinylated anti-GFP nanobody followed by streptavidin resulted in as rapid and extensive aggregation of sqh<sup>FRB-GFP</sup> as seen with our FRB-based technique (Figure 4, b–b''). This approach also resulted in the apparent loss of sqh activity in the injected region, as seen by both defects in ventral furrow formation (Figure 4, b–b''') and loss of circularity of the furrow canals (Figure 4, c and d; Supplemental Figure S2b). This technique is somewhat less robust than the AID2-based technique, which reduces sqh-GFP signal and blocks morphogenesis in all samples. The aggregation-based technique results in substantial aggregation in ~50% of samples: the phenotypes and effects on mechanics were only scored in samples in which aggregation was clearly apparent (see Figure 4 legend). We attribute this variability to increased sensitivity to the relative concentrations of the two components that are being injected. On the other hand, this approach is remarkably fast compared with AID2-based degrada-

tion; sqh<sup>FRB-GFP</sup> aggregation appears to occur completely within the ~5 min (Supplemental Movie 3). This allows us to examine the effects of sqh on tissue rheology while further reducing the possible action of compensatory downstream effects. We then performed ferrofluid-based measurements on embryos where myosin was depleted through aggregation and found that tissue mechanics again remained largely unaffected (Figure 3). Specifically, the percent recoil measured  $73.4 \pm 2.8$  SEM ( $n = 9$ ), while the relaxation time constant of the recoil had a value of  $50.6 \pm 3.5$  (SEM) seconds ( $n = 6$ ). In this way, this much more rapid technique for protein depletion corroborates our previous finding using the AID2 system.

## DISCUSSION

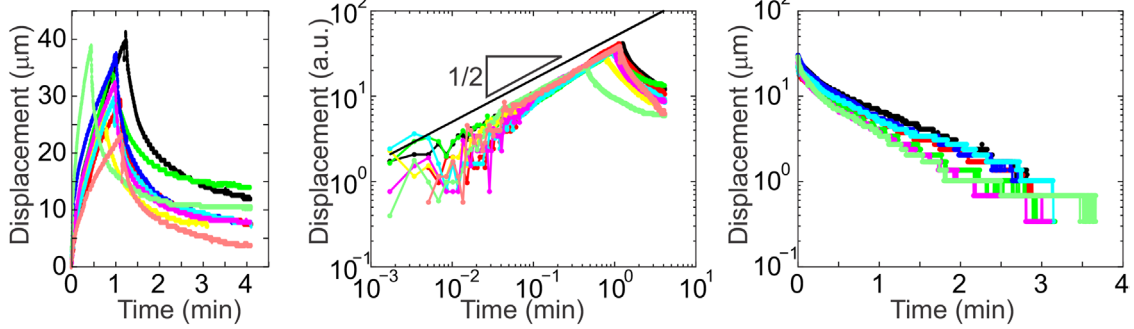
In this study, we used the AID2 degron technique and a novel sequestration approach to acutely inactivate the MRLC sqh in the cellularization stage *Drosophila* embryo and examine the effect on tissue material properties. We demonstrated that both techniques were very effective at depleting myosin activity, as seen by the resulting cellularization and ventral formation phenotypes. Strikingly, sqh depletion causes little to no change in tissue rheology. Specifically, we compared measurements reflecting the storage of elastic energy over time and the ratio of elasticity to viscosity, and found that neither was significantly altered.

Several studies have explored cell and tissue mechanics by measuring the deformations induced under some particular pattern of applied force (Thoumine and Ott, 1997; Bausch *et al.*, 1998; Hoffman *et al.*, 2006; Fernandez *et al.*, 2007; Bambardekar *et al.*, 2015; Doubrovinski *et al.*, 2017; D'Angelo *et al.*, 2019; Khalilgharibi *et al.*, 2019). However, the interpretation of these measurements is not always straightforward (Wu *et al.*, 2018). One complication comes in trying to disentangle the effects of passive properties versus active (i.e., energy-consuming) responses. Importantly, a meshwork that exhibits very low elasticity but is subjected to significant uniform active stress can exhibit mechanical responses very similar to a network with high elasticity and no stress present (Mulla *et al.*, 2019). In previous work in cellularization-stage *Drosophila* embryos, we found that tissue recoil after removal of force is nearly abolished in the presence of cytochalasin D, and we argued that the recoil should be interpreted as the passive elastic response of the actin cytoskeleton (Doubrovinski *et al.*, 2017). However, an alternative interpretation exists: the recoil is an active process. In our view, the most likely active process is myosin contractility, which is why we examined myosin loss of function in this study, although in principle other active contributions are conceivable. The results of the current study argue strongly against myosin contractility contributing to the recoil, and therefore provide support for the conclusion that the epithelium of cellularization-stage *Drosophila* embryo is highly elastic.

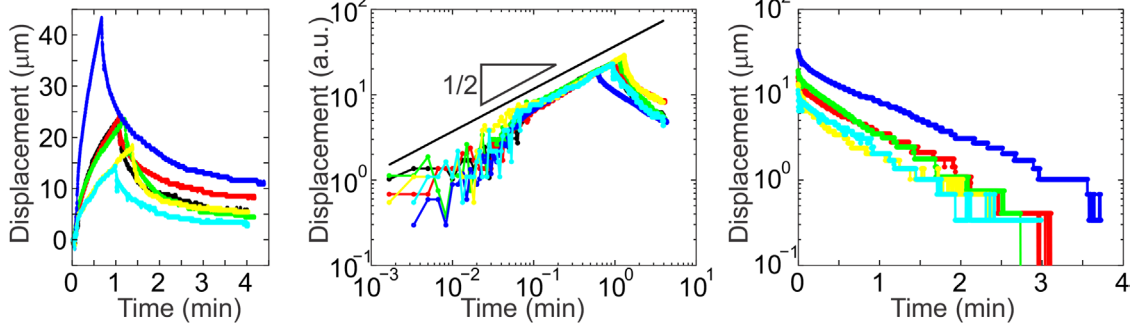
Beyond supporting the conclusion that this tissue exhibits strong passive elasticity, the results presented here also indicate that myosin activity has little to no influence on the strength of that elasticity. This is an important thing to establish in our system of interest, the cellularization stage *Drosophila* embryo, because experiments in other cells and tissues have variously shown stiffening (Chan *et al.*, 2015), softening (Martens and Radmacher, 2008), or no effect on elasticity (Van Citters *et al.*, 2006; Fernandez *et al.*, 2007) in response to myosin inhibition.

Because the experiments here involved specifically depleting the MRLC, we were probing the contribution of active myosin. This may not be identical to the contribution of the myosin complex overall. Work in other systems has suggested that the myosin heavy chain alone can act as an actin crosslinker that makes substantial contributions to elasticity (Xu *et al.*, 2001). In the future, it would be interesting

## Control



## AID2



## Aggregation assay

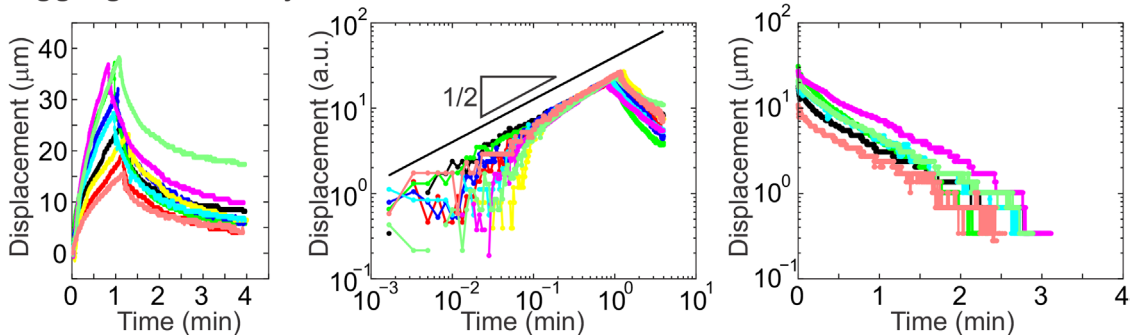


**FIGURE 3:** Quantification of tissue material properties after myosin depletion. Different color traces are repetitions of the same experiment in different embryos. Top panels show the measurements in the untreated (control) embryos. Middle panels correspond to embryos in which  $\text{sqh}^{\text{GFP-AID}}$  was depleted using the AID2 technique. Bottom panels correspond to embryos in which  $\text{sqh}^{\text{FRB-GFP}}$  was depleted using the nanobody-GFP aggregation-based technique. Left-most figures show the displacement of the ferrofluid droplet as a function of time. Middle figures represent the same data on a log-log plot. Right-most figures show plots of the recoil dynamics with logarithmic y-axis. Average values  $\pm$  SEM are given in the main text. Single-factor ANOVA failed to show a statistical difference among all three samples for the calculated relaxation time-constant ( $p = 0.11$ ) and percent recoil ( $p = 0.92$ ). Control  $n = 9$ , AID2  $n = 6$ , Aggregation assay  $n = 9$ .

to test whether myosin heavy chain acts similarly in this tissue, by targeting the non-muscle myosin 2 heavy chain zipper for degradation or sequestration and measuring the impact on rheology.

On the technical side, we have introduced two related novel techniques (based on FKBP-FRB and nanobody-GFP interactions) for very rapid sequestration of highly abundant proteins in the early embryo. Because GFP tags have been introduced into a large number of genes in the *Drosophila* genome (Morin *et al.*, 2001; Buszczak *et al.*, 2007; Quinones-Coello *et al.*, 2007; Nagarkar-Jaiswal *et al.*, 2015), the nanobody-GFP-based technique is immediately applicable to studying the role of those proteins in the embryo. Both techniques involve the injection of some components, which limits their

application, but are still accessible in a variety of key model systems such as tissue culture cells, oocytes, *Caenorhabditis elegans* germline, and other syncytial tissues. Although several techniques based on similar principles have been developed recently (Lee *et al.*, 2014; Qin *et al.*, 2017; Hernandez-Candia *et al.*, 2021; Yoshikawa *et al.*, 2021), both the rate and the degree of protein inactivation achieved by our method is significantly higher than in the previous studies. The rate of protein inactivation can be a critical factor in determining the direct role that a protein plays in a specific process. For example, if myosin is being depleted over the course of 40 min, it would be difficult to separate effects on cellularization (which occurs over  $\sim 40$  min) and ventral furrow formation (which occurs immediately

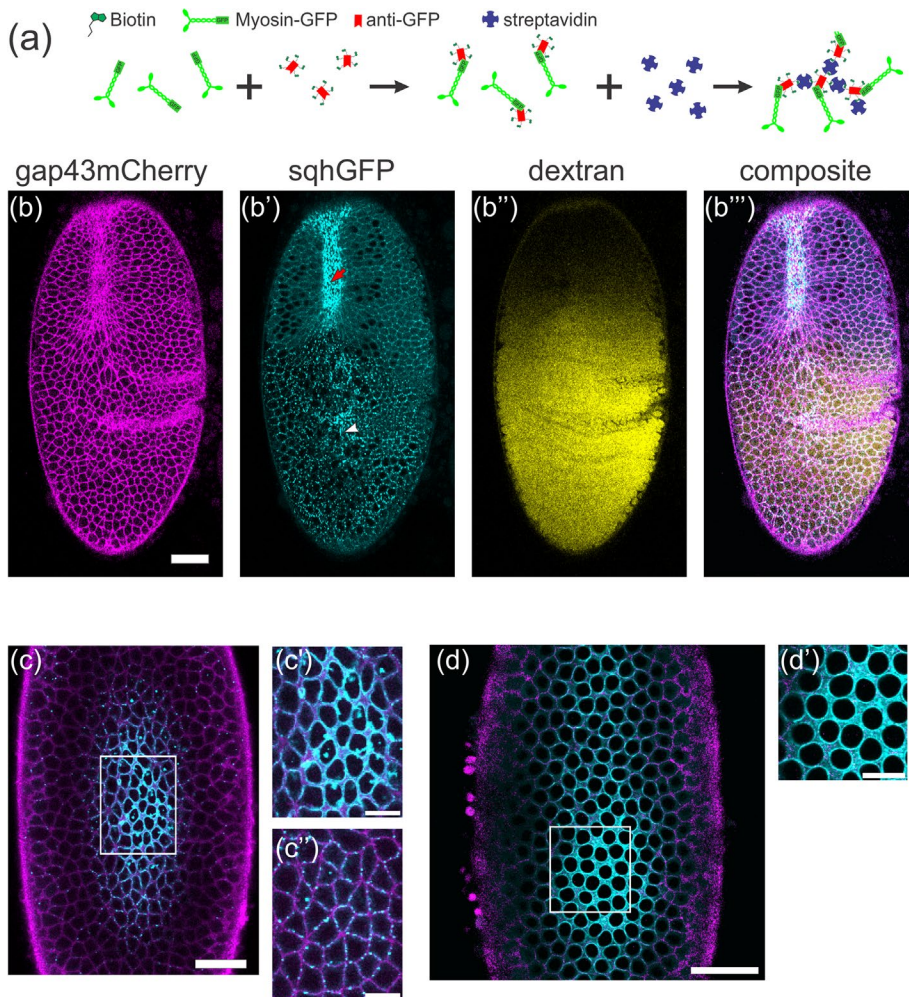


**FIGURE 4:** Aggregation-based assay for depletion of abundant proteins in the early *Drosophila* embryo. (a) Schematic illustrating the basis of the method (see text). (b–b''') A representative  $sqh^{FRB-GFP}$  embryo that has been injected with biotinylated anti-GFP nanobody and streptavidin. Yellow signal (b'') is coinjected dextran indicating distribution of the injected material. Gastrulation fails in the vicinity of the injection site. Red arrow indicates region with properly forming ventral furrow. White arrowhead indicates region where  $sqh^{FRB-GFP}$  forms aggregates; the ventral furrow fails to form in this region. Image was taken 5–10 min after the injection. Scalebar: 30  $\mu$ m. (c–c''). The same aggregation technique as in (b) performed at an earlier timepoint, during cellularization. Image was taken 5–10 min after the injection. Furrow canals lack the usual rounded shape, indicating loss of tension. (c') is a zoomed in image of the box indicated in (c). (c'') is from the same box, except 4  $\mu$ m closer to the surface; this image was included to show the aggregates, which are more obvious in this plane of section. (d). Uninjected control  $sqh^{FRB-GFP}$  embryo at the same stage as in (c) showing the typical rounded shape of the furrow canals for comparison. Note that the efficiency of this aggregation technique is not 100%. In the experiments examining ventral furrow formation, 5/10 embryos completely failed to form a ventral furrow, and three others exhibited delayed (>100 min) ventral furrow formation time compared with controls (<30 min). For comparison, single injection streptavidin controls consistently developed normally (10/10), and single injection biotinylated-GFP-nanobody controls consistently formed ventral furrows (10/10), although some (2/10) were delayed (~70 min). In the experiments examining furrow canals, substantial  $sqh^{FRB-GFP}$  aggregation and an accompanying severe effect on furrow canal morphology was obtained in 9/16 injected embryos, while 0/8 uninjected control embryos exhibited furrow canal defects. Scalebars: 25  $\mu$ m in (c) and (d); 10  $\mu$ m in (c', c'', and d').

afterwards over a time scale of ~15 min), because any treatment that would deplete myosin by the end of ventral furrow formation would also significantly reduce myosin levels during cellularization. However, a 5-min inactivation time would allow for these two processes

to be assessed separately. Regarding the degree of protein inactivation, we anticipate that many of the proteins that control tissue mechanical properties may be structural, rather than regulatory, in nature and therefore present in high concentration. A highly efficient method of depletion is therefore key to understanding how such proteins contribute to tissue mechanics. More generally, we envision that our approach of combining acute protein degradation or sequestration with rheological measurements will find additional applications in many other systems, and aid in dissecting the contributions of individual proteins to material properties in living biological systems.

## MATERIALS AND METHODS

[Request a protocol](#) through *Bio-protocol*.

### Plasmid construction

The  $gap43\_mCherry\_pCaSpeR4$  plasmid was generated by inserting a sequence encoding the  $gap43$  tag (the first 20 amino acids of rat  $gap43$ ) translationally fused to mCherry between the NotI and XbaI sites of Tubp-Gal80 in pCaSpeR4 (a gift from Liqun Luo; Addgene plasmid # 17748; <http://n2t.net/addgene:17748>; RRID:Addgene\_17748; Lee and Luo, 1999). This eliminated the Gal80 sequence and resulted in a plasmid with  $gap43$ -mCherry downstream of the tubulin promoter.

The mat-Gal4- $sqh$ UTR plasmid was generated by PCR amplification of the Gal4 coding sequence from pPac-Pl-mCD8-D2A-Gal4 (a gift from Benjamin White, Addgene plasmid # 39457; <http://n2t.net/addgene:39457>; RRID:Addgene\_39457; Diao and White, 2012). Primers used included a 5' NheI site and Kozak sequence (ATCAAC) and a 3' NotI site. The PCR product was inserted it into NheI/NotI cut  $\alpha$ Tub67c\_MCS\_ $sqh$ UTR pBABR (a gift from Shelby Blythe).

The pUASP-attB-TIR2-F74G plasmid was generated by synthesizing the TIR1-F74G sequence, along with a 5' Kozak sequence and 3' linker sequence (VDSGSAASG) plus HA tag, and inserting this into UASP-attB (DGRC Stock 1358; <https://dgrc.bio.indiana.edu/stock/1358>; RRID:DGRC\_1358) between NotI and XbaI. The TIR1-F74G sequence was a gift from Masato Kanemaki (Addgene plasmid # 140730; <http://n2t.net/addgene:140730>; RRID:Addgene\_140730; Yesbolatova et al., 2020).

The  $sqh\_GFP\_FRB\_donor$  plasmid was generated by inserting synthesized DNA between the two EcoRI sites of ScarlessDsRed\_pHD-2xHA (a gift from Kate O'Connor-Giles, Addgene plasmid # 80822; <http://n2t.net/addgene:80822>; RRID:Addgene\_80822). The inserted DNA contained these elements in order: a 900 base pair homology arm

derived from the *sqh* genomic sequence and ending with the final *sqh* coding exon; a linker encoding DYKEPVAT; GFP(S65T); FRB; a stop codon; and a 900 base pair homology arm corresponding to the genomic sequence downstream of the *sqh* coding region.

The *sqh*-GFPaid\_v2 plasmid was also generated by inserting synthesized DNA into the ScarlessDsRed\_pHD-2xHA backbone between the two *EcoRI* sites. The inserted DNA is the same as in the *sqh*\_GFP\_FRB\_donor plasmid with two exceptions: the sequence encoding AID (from GenBank NM\_100306.4) was substituted for FRB, and the first homology arm including a single, silent A-to-G change ten bases before its end to mutate the PAM site targeted by one of the guide RNAs.

The two guide RNA-expressing plasmids used for modification of the *sqh* genomic locus were designed using the tool at <https://flycrisper.org/target-finder> (Gratz *et al.*, 2014). The following sense/antisense pairs oligos were annealed separately and ligated into the *BbsI* sites of pU6-*BbsI*-*chiRNA* (Gratz *et al.*, 2013) 194:1029): guide1-sense: CTTTCGCTGGCTAGTGAATCGACTGC;

guide1-antisense: AAACGCAGTCGATTCACTAGCCAGC; guide2-sense: CTTTCGTAAGCACGGTGCCAAGGACA; and guide2-antisense: AAACGTCTCTGGCACCGTGCTTAC.

pET\_FRB\_Dark Cherry\_1xNano encodes a fusion protein containing 6xHis tag, dark mCherry, and anti-GFP nanobody sequences. The dark mCherry sequence was created by making a Y-to-G mutation in the chromophore. The GFP-nanobody sequence was a gift from Kazuhisa Nakayama (Addgene plasmid # 61838; <http://n2t.net/addgene:61838>; RRID:Addgene\_61838; Katoh *et al.*, 2015). pET\_FKBP\_mCherry encodes a fusion protein containing 6xHis tag, FRB, and mCherry sequences. pET\_FRB\_Dark Cherry\_1xNano and pET\_FKBP\_mCherry plasmids were constructed from pET28 FRB-ferritin and pET28 FKBP-ferritin respectively (both kind gifts of Zoher Gueroui; Ducasse *et al.*, 2017). The complete annotated sequences are listed in the supplement.

## Fly stocks

The genotype used for AID-degron experiments was *sqh*<sup>GFP-AID</sup>, *gap43-mCherry/sqh*<sup>AX3</sup>; +; *mat-GAL4*<sup>89E11</sup>, *mat-GAL4*<sup>15</sup>/*UASp-TIR1-F74G*<sup>VK00027</sup>, *UASp-TIR1-F74G*<sup>attP2</sup>. For aggregation experiments, the genotype used was *sqh*<sup>FRB-GFP</sup>; +; *gap43mCherry/TM3*, *Sb*. The control line used to measure background green autofluorescence in Figure 1a was *w*; +; *gap43mCherry/TM3*, *Sb*.

Bloomington *Drosophila* Stock Center was the source of *mat-GAL4*<sup>15</sup> (RRID:BDSC\_80361) and *sqh*<sup>AX3</sup> (RRID:BDSC\_25712). The *gap43-mCherry* (membrane-mCherry) on the third chromosome was a gift from Adam Martin (Martin *et al.*, 2010).

Flies with *gap43-mCherry* on the first chromosome were created by injection of the *gap43\_mCherry\_pCaSpeR4* plasmid into fly embryos using P-element mediated insertion; progeny were screened for X chromosome transformants. *mat-GAL4*<sup>89E11</sup> flies were created by injection of the *mat-Gal4-sqhUTR* plasmid into Rainbow line 35569 (genotype: *y*<sup>1</sup> *w*<sup>[\*]</sup> *P**[y(+7.7)]* = *nos-phiC31int.NLS X*; +; *PBac**[y(+)]attP-9A* *VK00027*). *UASp-TIR1-F74G*<sup>VK00027</sup> and *UASp-TIR1-F74G*<sup>attP2</sup> flies were created by injection of the *pUASP-attB-TIR2-F74G* plasmid into the Rainbow lines 35569 (genotype listed above) and R8622 (genotype: *M**{vas-int.DmZH-2A}*; +; *P**{CaryP attP2}*), respectively.

Flies carrying *sqh*<sup>FRB-GFP</sup> and *sqh*<sup>GFP-AID</sup> were generated by CRISPR-based modification to the C-terminus of *sqh* at its endogenous locus. In both cases, flies of genotype *y*,*sc,v*; +/+; *nos-Cas9 attP2* were injected with a mixture of 250-ng/  $\mu$ l donor plasmid and 20 ng/  $\mu$ l of each guide plasmid in water. The same two guide plasmids (described in the Plasmids section) were used in both cases. The donor plasmids for *sqh*<sup>FRB-GFP</sup> and *sqh*<sup>GFP-AID</sup>, called *sqh*\_GFP\_

*FRB\_donor* and *sqh*-GFPaid\_v2, respectively, are also described in that section. Progeny of injected flies were screened for successful modification of the *sqh* genomic locus by a combination of screening for GFP fluorescence in dissected egg chambers and genomic PCR with sequencing. The *sqh*<sup>FRB-GFP</sup> flies generated by this method incorporated the full-length FRB-GFP sequence from the donor plasmid. Only one *sqh*<sup>GFP-AID</sup> line was found screening by GFP fluorescence, and genomic sequencing revealed that while the entire GFP sequence was incorporated, the AID sequence incorporated was truncated, followed by a small inserted sequence, then the 3' UTR of *sqh*. The final result is a shortened AID tag (M1-K124) followed by the amino-acid sequence DEQ. Because this shortened tag included a functional shortened mini-AID sequence (Kubota *et al.*, 2013; Morawska and Ulrich, 2013; Brosh *et al.*, 2016), we tested and successfully used this line in experiments.

All injections for generating transgenic flies were done by Rainbow Transgenic Flies.

## Protein purification and biotinylation

Anti-GFP-nanobody protein was produced from the plasmid pET\_FRB\_Dark Cherry\_1xNano. The final fusion protein includes FRB (FKBP-rapamycin binding) and dark mCherry domains, but these do not play specific functional roles in the experiments presented here (beyond providing more potential biotinylation sites), so we refer to this protein as "anti-GFP nanobody" for clarity. FKBP-mCherry protein (in Supplemental Figure S1) was produced from the plasmid pET\_FKBP\_mCherry.

To produce the protein, expression plasmids were transformed into *E. coli* BL21(DE3) cells (ThermoFisher Scientific cat# C600003). Overnight cultures were used to inoculate flasks containing 500-ml lysogeny broth with 50- $\mu$ g/ml kanamycin, and flasks were shaken at 37°C until cultures reached an OD<sub>600</sub> of 0.6–0.8. Isopropyl  $\beta$ -D-1-thiogalactopyranoside (Invitrogen #15529-019) was added at a final concentration of 1 mM and the cultures shaken at 26°C for 3 h. Cells were harvested by centrifugation and pellets were frozen at –80°C for later use. Thawed cell lysates were resuspended in suspension buffer (100-mM NaCl, 4-mM Tris pH 7.5, supplemented with cOmplete, EDTA-free Protease inhibitor cocktail, Sigma cat # 11873580001). Cells were lysed at 4°C by incubating with 0.002  $\mu$ g/ml lysozyme (Sigma L6876) for 10 min, sonicated for 4 10-s pulses in a MisonX 3000 ultrasonicator, and incubated with 0.05-mg/ml Deoxyribonuclease I (Sigma D4527), 12.5- $\mu$ M MgCl<sub>2</sub>, and 1.25% Triton X-100. Lysate was cleared by centrifugation at 24,000 g for 30 min.

Proteins were His-tagged, and so were purified using Ni-NTA agarose beads (ThermoFisher Scientific cat# R90101) essentially according to manufacturer's instructions. Protein recovery was maximized by adjusting the concentration of imidazole (Sigma cat# I5513-5G) as follows: Ni-NTA agarose beads (ThermoFisher Scientific cat# R90101) were resuspended in 0mM Imidazole buffer (50-mM sodium phosphate; pH 8.0; 300-mM NaCl) before incubating with cleared lysate. Beads were washed twice with 0-mM Imidazole buffer, then twice with 10-mM Imidazole buffer (50-mM sodium phosphate pH 8.0; 300-mM NaCl; 10-mM imidazole). 500  $\mu$ l fractions were eluted with 250-mM Imidazole buffer (50-mM sodium phosphate pH 8.0; 300-mM NaCl; 250-mM imidazole), and protein concentration was measured by OD<sub>280</sub>. Fractions of at least 1-mg/ml protein were combined and dialyzed into PBS using 10K MWCO dialysis cassettes. For the data presented in this paper, the concentration of FKBP-Cherry as measured before biotinylation was 12 mg/ml, and the concentration of anti-GFP nanobody as measured before biotinylation was 6.4 mg/ml, but a range of concentrations used in other experiments gave similar results.

To biotinylate the proteins, Biotinamidocaproate N-Hydroxy-succinimide ester (Sigma # B2643) was dissolved to 38.5 mM in N,N-dimethylformamide (Sigma-Aldrich #227056) then combined with the protein solution in a 15:1 (biotinylation reagent: protein) molar ratio. After incubation for 45 min at room temperature, the protein was dialyzed into PBS to remove unconjugated biotin and stored at 4°C.

### Embryo injections

Embryos were collected on grape agar plates and stage-selected under Halocarbon 27 oil (Sigma or Halocarbon InfinX), dechorionated in bleach, then washed with water. Embryos were then mounted ventral side down along a line of embryo glue (double-sided scotch tape extract in heptane) on a glass coverslip. The coverslip was placed in a closed plastic container with drierite, and allowed to dry for 15 min. Embryos were then covered in Halocarbon 700 oil (Sigma) to prevent further drying. Embryos were injected laterally, near the anterior end.

For AID degenon experiments, embryos were injected with 50-mM 5-Ph-IAA-AM in DMSO. For aggregation experiments, embryos were first injected with biotinylated anti-GFP nanobody (or biotinylated FKBP-mCherry mixed with equimolar rapamycin, centrifuged to clear, in Supplemental Figure S1) solution on one side of the embryo. The coverslip slip was then rotated 180°, and a streptavidin mixture was injected laterally, directly opposite the first injection. This mixture was prepared by mixing 20-mg/ml streptavidin (Roche 11721674001) in a 2:1 ratio with 10-mg/ml Alexa Fluor 647 conjugated dextran (ThermoFisher Scientific D22914), to aid in visualizing injection into the embryo. Ferrofluid injections, if any, were performed last. All injections were facilitated using a FemtoJet 5247 Microinjector (Eppendorf).

To prepare needles for protein or 5-Ph-IAA injection, glass capillaries (Sutter Instruments, #BF100-78-10) were pulled using a micro-pipette puller (Sutter Model P-2000) using the following settings: Heat = 350, Fil = 6, Vel = 30, Del = 110, and Pul = 120. Needles were loaded using microloader tips (Eppendorf 5242 956.003). Finally, the needle was gently broken by pressing the tip against the side of a coverslip after loading to open the tip.

### Ferrofluid experiments

Ferrofluid injections and rheological measurements were done as previously described in (Dobrovinski *et al.* 2017). Borosilicate glass capillaries with an inner diameter of 0.5 mm (Sutter BF100-50-10) were pulled into injection needles using a Sutter P-2000 pipette puller with the following settings: Heat = 380, Fil = 4, Vel = 20, Del = 128, and Pul = 120. Pulled needles were beveled using an EG-45 microgrinder (Narishige), then loaded with ferrofluid (Apexmagnets Ferrofluid Magnetic Liquid – 8 oz) for injection into embryos. External force was applied to ferrofluid droplets using a permanent magnet mounted on a manual translation stage. In all AID2 experiments, pulling was done on the side of the embryo opposite to the site of injection, to minimize complications from any possible tissue damage. Because effects of protein aggregation were sometimes more local, the site of pulling was adjusted to be in a region of the embryo with substantial sqh-GFP aggregation.

### Imaging

Imaging was done on a Zeiss LSM 700. A Plan-Apochromat 20x/0.8 M27 objective was used for ferrofluid experiments; an EC Plan-Neofluar 40x/1.30 oil DIC M27 objective was used for all other experiments.

### ACKNOWLEDGMENTS

Plasmids obtained from the Drosophila Genomics Resource Center (National Institutes of Health [NIH] Grant 2P40OD010949) and stocks obtained from the Bloomington Drosophila Stock Center (NIH P400D018537) were used in this study. Research reported in this publication was supported by NIH, National Institute of General Medical Sciences award 1R01GM134207; NIH, National Institute for Child Health and Human Development award 1R21HD105189; Robert A. Welch Foundation award I-1950-20180324.

### REFERENCES

- Bambardekar K, Clement R, Blanc O, Chardes C, Lenne PF (2015). Direct laser manipulation reveals the mechanics of cell contacts in vivo. *Proc Natl Acad Sci USA* 112, 1416–1421.
- Bausch AR, Ziemann F, Boulbitch AA, Jacobson K, Sackmann E (1998). Local measurements of viscoelastic parameters of adherent cell surfaces by magnetic bead microrheometry. *Biophys J* 75, 2038–2049.
- Behrndt M, Salbreux G, Campinho P, Hauschild R, Oswald F, Roensch J, Grill SW, Heisenberg CP (2012). Forces driving epithelial spreading in zebrafish gastrulation. *Science* 338, 257–260.
- Bence M, Jankovics F, Lukacsovich T, Erdelyi M (2017). Combining the auxin-inducible degradation system with CRISPR/Cas9-based genome editing for the conditional depletion of endogenous Drosophila melanogaster proteins. *FEBS J* 284, 1056–1069.
- Bendix PM, Koenderink GJ, Cuvelier D, Dogic Z, Koeleman BM, Briehner WM, Field CM, Mahadevan L, Weitz DA (2008). A quantitative analysis of contractility in active cytoskeletal protein networks. *Biophys J* 94, 3126–3136.
- Blankenship JT, Backovic ST, Sanny JSP, Weitz O, Zallen JA (2006). Multicellular rosette formation links planar cell polarity to tissue morphogenesis. *Dev Cell*, 11, 459–470.
- Brosh R, Hrynyk I, Shen J, Waghay A, Zheng N, Lemischka IR (2016). A dual molecular analogue tuner for dissecting protein function in mammalian cells. *Nat Commun* 7, 11742.
- Buszczak M, Paterno S, Lighthouse D, Bachman J, Planck J, Owen S, Skora AD, Nystul TG, Ohlstein B, Allen A, *et al.* (2007). The carnegie protein trap library: a versatile tool for Drosophila developmental studies. *Genetics* 175, 1505–1531.
- Campas O, Mammoto T, Hasso S, Sperling RA, O’Connell D, Bischof AG, Maas R, Weitz DA, Mahadevan L, Ingber DE (2014). Quantifying cell-generated mechanical forces within living embryonic tissues. *Nat Methods* 11, 183–189.
- Campos-Ortega JA, Hartenstein V (1985). *The Embryonic Development of Drosophila melanogaster*, Heidelberg, Berlin: Springer.
- Chan CJ, Ekpenyong AE, Golfier S, Li W, Chalut KJ, Otto O, Elgeti J, Guck J, Lautenschlager F (2015). Myosin II activity softens cells in suspension. *Biophys J* 108, 1856–1869.
- Chen P, Ostrow BD, Tafuri SR, Chisholm RL (1994). Targeted disruption of the Dictyostelium RMLC gene produces cells defective in cytokinesis and development. *J Cell Biol* 127, 1933–1944.
- D’angelo A, Dierkes K, Carolis C, Salbreux G, Solon J (2019). In vivo force application reveals a fast tissue softening and external friction increase during early embryogenesis. *Curr Biol* 29, 1564–1571. e6.
- Davidson LA (2017). Mechanical design in embryos: mechanical signalling, robustness and developmental defects. *Philos Trans R Soc Lond B Biol Sci* 372, 20150516.
- Diao F, White BH (2012). A novel approach for directing transgene expression in Drosophila: T2A-Gal4 in-frame fusion. *Genetics* 190, 1139–1144.
- Dobrovinski K, Swan M, Polyakov O, Wieschaus EF (2017). Measurement of cortical elasticity in Drosophila melanogaster embryos using ferrofluids. *Proc Natl Acad Sci U S A* 114, 1051–1056.
- Dubey S, Bhembre N, Bodas S, Veer S, Ghose A, Callan-Jones A, Pullarkat P (2020). The axonal actin-spectrin lattice acts as a tension buffering shock absorber. *Elife* 9, e51772.
- Ducasse R, Wang WA, Navarro MGJ, Debons N, Colin A, Gautier J, Guigner JM, Guyot F, Gueroui Z (2017). Programmed self-assembly of a biochemical and magnetic scaffold to trigger and manipulate microtubule structures. *Sci Rep* 7, 11344.
- Fernandez P, Heymann L, Ott A, Aksel N, Pullarkat PA (2007). Shear rheology of a cell monolayer. *N J Phys* 9, 419.
- Gardel ML, Kasza KE, Brangwynne CP, Liu JY, Weitz DA (2008). Chapter 19: mechanical response of cytoskeletal networks. *Methods Cell Biol* 89, 487–519.

- Goldstein LS, Gunawardena S (2000). Flying through the drosophila cytoskeletal genome. *J Cell Biol* 150, F63–F68.
- Gratz SJ, Cummings AM, Nguyen JN, Hamm DC, Donohue LK, Harrison MM, Wildonger J, O’connor-Giles KM (2013). Genome engineering of *Drosophila* with the CRISPR RNA-Guided Cas9 nuclease. *Genetics* 194, 1029–1035.
- Gratz SJ, Ukken FP, Rubinstein CD, Thiede G, Donohue LK, Cummings AM, O’connor-Giles KM (2014). Highly specific and efficient CRISPR/Cas9-catalyzed homology-directed repair in *Drosophila*. *Genetics* 196, 961–971.
- Hernandez-Candia CN, Pearce S, Tucker CL (2021). A modular tool to query and inducibly disrupt biomolecular condensates. *Nat Commun* 12, 1809.
- Hernandez-Vega A, Marsal M, Pouille PA, Tosi S, Colombelli J, Luque T, Navajas D, Pagonabarraga I, Martin-Blanco E (2017). Polarized cortical tension drives zebrafish epiboly movements. *EMBO J* 36, 25–41.
- Hoffman BD, Massiera G, Citters KMV, Crocker JC (2006). The consensus mechanics of cultured mammalian cells. *Proc Natl Acad Sci USA* 103, 10259–10264.
- Janmey PA, Hvidt S, Kas J, Lerche D, Maggs A, Sackmann E, Schliwa M, Stossel TP (1994). The mechanical-properties of actin gels. Elastic modulus and filament motions. *J Biol Chem* 269, 32503–32513.
- Joanny JF, Prost J (2009). Active gels as a description of the actin-myosin cytoskeleton. *HFSP J* 3, 94–104.
- Karess RE, Chang XJ, Edwards KA, Kulkarni S, Aguilera I, Kiehart DP (1991). The regulatory light chain of nonmuscle myosin is encoded by spaghetti-squash, a gene required for cytokinesis in *Drosophila*. *Cell* 65, 1177–1189.
- Katoh Y, Nozaki S, Hartanto D, Miyano R, Nakayama K (2015). Architectures of multisubunit complexes revealed by a visible immunoprecipitation assay using fluorescent fusion proteins. *J Cell Sci* 128, 2351–2362.
- Keller R (2012). Developmental biology. Physical biology returns to morphogenesis. *Science* 338, 201–203.
- Khalilgharibi N, Fouchard J, Asadipour N, Barrientos R, Duda M, Bonfanti A, Yonis A, Harris A, Mosaffa P, Fujita Y, et al. (2019). Stress relaxation in epithelial monolayers is controlled by the actomyosin cortex. *Nat Phys* 15, 839–847.
- Kiehart DP, Crawford JM, Aristotelous A, Venakides S, Edwards GS (2017). Cell sheet morphogenesis: dorsal closure in *Drosophila melanogaster* as a model system. *Annu Rev Cell Dev Biol* 33, 169–202.
- Koenderink GH, Dogic Z, Nakamura F, Bendix PM, Mackintosh FC, Hartwig JH, Stossel TP, Weitz DA (2009). An active biopolymer network controlled by molecular motors. *Natl Acad Sci USA* 106, 15192–15197.
- Kubota T, Nishimura K, Kanemaki MT, Donaldson AD (2013). The Elg1 replication factor C-like complex functions in PCNA unloading during DNA replication. *Mol Cell* 50, 273–280.
- Lee S, Park H, Kyung T, Kim NY, Kim S, Kim J, Heo WD (2014). Reversible protein inactivation by optogenetic trapping in cells. *Nat Methods* 11, 633–636.
- Lee T, Luo L (1999). Mosaic analysis with a repressible cell marker for studies of gene function in neuronal morphogenesis. *Neuron* 22, 451–461.
- Lenne PF, Trivedi V (2022). Sculpting tissues by phase transitions. *Nat Commun* 13, 664.
- Martens JC, Radmacher M (2008). Softening of the actin cytoskeleton by inhibition of myosin II. *Pflugers Arch* 456, 95–100.
- Martin AC, Gelbart M, Fernandez-Gonzalez R, Kaschube M, Wieschaus EF (2010). Integration of contractile forces during tissue invagination. *J Cell Biol* 188, 735–749.
- Martin AC, Kaschube M, Wieschaus EF (2009). Pulsed contractions of an actin-myosin network drive apical constriction. *Nature* 457, 495–499.
- Mayer M, Depken M, Bois JS, Julicher F, Grill SW (2010). Anisotropies in cortical tension reveal the physical basis of polarizing cortical flows. *Nature* 467, 617–621.
- Mongera A, Rowghanian P, Gustafson HJ, Shelton E, Kealhofer DA, Carn EK, Serwane F, Lucio AA, Giammona J, Campas O (2018). A fluid-to-solid jamming transition underlies vertebrate body axis elongation. *Nature* 561, 401–405.
- Morawska M, Ulrich HD (2013). An expanded tool kit for the auxin-inducible degron system in budding yeast. *Yeast* 30, 341–351.
- Morin X, Daneman R, Zavortink M, Chia W (2001). A protein trap strategy to detect GFP-tagged proteins expressed from their endogenous loci in *Drosophila*. *Proc Natl Acad Sci USA* 98, 15050–15055.
- Mulla Y, Mackintosh FC, Koenderink GH (2019). Origin of slow stress relaxation in the cytoskeleton. *Phys Rev Lett* 122, 218102.
- Munster S, Jain A, Mietke A, Pavlopoulos A, Grill SW, Tomancak P (2019). Attachment of the blastoderm to the vitelline envelope affects gastrulation of insects. *Nature* 568, 395–399.
- Nagarkar-Jaiswal S, Lee PT, Campbell ME, Chen K, Anguiano-Zarate S, Gutierrez MC, Busby T, Lin WW, He Y, Schulze KL, et al. (2015). A library of MiMiCs allows tagging of genes and reversible, spatial and temporal knockdown of proteins in *Drosophila*. *Elife* 4, e05338.
- Natsume T, Kanemaki MT (2017). Conditional degrons for controlling protein expression at the protein level. *Annu Rev Genet* 51, 83–102.
- Negishi T, Kitagawa S, Horii N, Tanaka Y, Haruta N, Sugimoto A, Sawa H, Hayashi KI, Harata M, Kanemaki MT (2022). The auxin-inducible degron 2 (AID2) system enables controlled protein knockdown during embryogenesis and development in *Caenorhabditis elegans*. *Genetics* 220, iyab218.
- Nishimura K, Fukagawa T, Takisawa H, Kakimoto T, Kanemaki M (2009). An auxin-based degron system for the rapid depletion of proteins in nonplant cells. *Nat Methods* 6, 917–922.
- Pegoraro AF, Janmey P, Weitz DA (2017). Mechanical properties of the cytoskeleton and cells. *Cold Spring Harb Perspect Biol* 9, a022038.
- Qin X, Park BO, Liu JY, Chen B, Choemel-Cadamuro V, Belguise K, Heo WD, Wang XB (2017). Cell-matrix adhesion and cell-cell adhesion differentially control basal myosin oscillation and *Drosophila* egg chamber elongation. *Nat Commun* 8, 14708.
- Quinones-Coello AT, Petrella LN, Ayers K, Melillo A, Mazzalupo S, Hudson AM, Wang S, Castiblanco C, Buszczak M, Hoskins RA, Cooley L (2007). Exploring strategies for protein trapping in *Drosophila*. *Genetics* 175, 1089–1104.
- Royou A, Field C, Sisson JC, Sullivan W, Karess R (2004). Reassessing the role and dynamics of nonmuscle myosin II during furrow formation in early *Drosophila* embryos. *Mol Biol Cell* 15, 838–850.
- Serwane F, Mongera A, Rowghanian P, Kealhofer DA, Lucio AA, Hockenbery ZM, Campas O (2017). In vivo quantification of spatially varying mechanical properties in developing tissues. *Nat Methods* 14, 181–186.
- Thoumine O, Ott A (1997). Time scale dependent viscoelastic and contractile regimes in fibroblasts probed by microplate manipulation. *J Cell Sci* 110, 2109–2116.
- Van Citters KM, Hoffman BD, Massiera G, Crocker JC (2006). The role of F-actin and myosin in epithelial cell rheology. *Biophys J* 91, 3946–3956.
- Vuong-Breder TTK, Amar MB, Pontabry J, Labouesse M (2017). The interplay of stiffness and force anisotropies drives embryo elongation. *Elife* 6, e23866.
- Wu PH, Aroush DRB, Asnacios A, Chen WC, Dokukin ME, Doss BL, Durand-Smet P, Ekpenyong A, Guck J, Guz NV, et al. (2018). A comparison of methods to assess cell mechanical properties. *Nat Methods* 15, 491–498.
- Xu K, Zhong G, Zhuang X (2013). Actin, spectrin, and associated proteins form a periodic cytoskeletal structure in axons. *Science* 339, 452–456.
- Xu XS, Lee E, Chen T, Kuczmarski E, Chisholm RL, Knecht DA (2001). During multicellular migration, myosin II serves a structural role independent of its motor function. *Dev Biol* 232, 255–264.
- Yesbolatova A, Saito Y, Kitamoto N, Makino-Itou H, Ajima R, Nakano R, Nakaoka H, Fukui K, Gamo K, Tominari Y, et al. (2020). The auxin-inducible degron 2 technology provides sharp degradation control in yeast, mammalian cells, and mice. *Nat Commun* 11, 5701.
- Yoshikawa M, Yoshii T, Ikuta M, Tsukiji S (2021). Synthetic protein condensates that inducibly recruit and release protein activity in living cells. *J Am Chem Soc* 143, 6434–6446.